Barker, P.F., Camerlenghi, A., Acton, G.D., and Ramsay, A.T.S. (Eds.)
Proceedings of the Ocean Drilling Program, Scientific Results Volume 178

14. Data Report: The Magnetic Mineral Assemblage of Hemipelagic Drifts, ODP Site 1096[1]

Stefanie A. Brachfeld,[2] Y. Guyodo,[3] and G.D. Acton[4]

INTRODUCTION

During Ocean Drilling Program (ODP) Leg 178, we drilled three sites on sediment drifts deposited on the continental rise on the western margin of the Antarctic Peninsula. These hemipelagic drifts were targeted for their potential to preserve a continuous record of the behavior of the West Antarctic Ice Sheet over the last 10 m.y. It has been proposed that drift development is linked to advances and retreats of the Antarctic continental ice sheet (Pudsey and Camerlenghi, 1998, and references therein; Barker, Camerlenghi, Acton, et al., 1999). However, the sediment is characterized by a very low carbonate content, with foraminifers restricted to very narrow intervals. This lack of carbonate precludes the construction of a $\delta^{18}O$ or $CaCO_3$ stratigraphy, depriving these sites of an important chronologic tool and global ice volume proxy.

As an alternative, we have compiled a rock-magnetic data set. Rock-magnetic investigations serve several purposes:

1. Continuous records of variations in the intensity of the geomagnetic field have been demonstrated to be powerful correlation and dating tools for the past 800 k.y. (Guyodo and Valet, 1996, 1999; Laj et al., 2000). The use of geomagnetic field paleointensity as a dating tool at this site requires the removal of climatic influences on the recording assemblage. Toward that end, rock-magnetic investigations have been carried out to assess the "uniformity" of the magnetic mineral assemblage (see Tauxe, 1993).
2. Rock-magnetic parameters contain information regarding the source material and processes controlling the erosion, transport,

[1]Brachfeld, S.A., Guyodo, Y., and Acton, G.D., 2001. Data report: The magnetic mineral assemblage of hemipelagic drifts, ODP Site 1096. *In* Barker, P.F., Camerlenghi, A., Acton, G.D., and Ramsay, A.T.S. (Eds.), *Proc. ODP, Sci. Results,* 178, 1–12 [Online]. Available from World Wide Web: <http://www-odp.tamu.edu/publications/178_SR/VOLUME/CHAPTERS/SR178_14.PDF>. [Cited YYYY-MM-DD]
[2]Byrd Polar Research Center, Ohio State University, 108 Scott Hall, 1090 Carmack Road, Columbus OH 43210, USA. **brachfeld.2@osu.edu**
[3]Department of Geological Sciences, University of Florida, 241 Williamson Hall, PO Box 112120, Gainesville FL 32611-2120, USA.
[4]Ocean Drilling Program, Texas A&M University, 1000 Discovery Drive, College Station TX 77845-9547, USA.

Initial receipt: 26 January 2001
Acceptance: 23 May 2001
Web publication: 9 August 2001
Ms 178SR-233

and deposition of the sediment. Therefore, rock-magnetic parameters can be a valuable tool for both chronology and paleoclimate applications.

SITE DESCRIPTION AND SAMPLES

We focus on ODP Leg 178 Site 1096, which was drilled on the crest of Drift 7 (67°34.0086′S, 76°57.7936′W). The section was cored down to ~120 meters below seafloor (mbsf) via advanced hydraulic piston coring (APC) and extended down to 608 mbsf by extended core barrel (XCB) coring. The base of the section has been dated at ~4.7 Ma, based on magnetostratigraphy and biostratigraphy. Subsamples were collected at a frequency of two per section in Hole 1096A and one per section in Holes 1096B and 1096C, giving us a temporal sampling interval of ~4.7 k.y. in the APC cores (linear sedimentation rate [LSR] = 8 cm/k.y.) and 8.3 k.y. in the XCB cores (LSR = 18 cm/k.y.). Our purpose here is to present the results of mineralogical investigations, providing ground truth for high-resolution paleomagnetic and environmental proxies derived from U-channel samples.

EXPERIMENTAL METHODS

Whole-core magnetic susceptibility (k) was measured on board the *JOIDES Resolution* during ODP Leg 178 using an automated multisensor track (Barker, Camerlenghi, Acton, et al., 1999). Subsamples were freeze-dried for magnetic granulometry analyses performed at the Institute for Rock Magnetism at the University of Minnesota. Hysteresis parameters were measured on a Princeton Measurements Corp. microvibrating sample magnetometer. Low-temperature (20 to 300 K) remanence and susceptibility measurements were made using a Quantum Design MPMS-XL susceptometer.

RESULTS

We carried out rock magnetic analyses that probed the composition, particle size, and concentration of the magnetic mineral assemblage. Many magnetic minerals undergo magnetic order–disorder transitions and crystallographic phase transitions at temperatures ranging from 10 to 1000 K that can be used as diagnostic indicators of a mineral's presence or absence (see Dunlop and Özdemir, 1997, for full discussion). We used low-temperature (20 to 300 K) measurements to determine the composition of the magnetic mineral assemblage. Low-temperature analyses consisted of a pair of measurements. First, a sample was cooled in zero applied field from 300 to 20 K, given a 2.5-T saturation remanence (M_R) at 20 K, and M_R was then measured during warming to 300 K. The sample was then cooled back down to 20 K, this time in the presence of a 2.5-T applied field, and M_R was remeasured during warming to 300 K. This zero field cooled (ZFC) and field cooled (FC) pair of measurements, described in detail in Moskowitz et al. (1993) has proven useful in evaluating magnetic domain state and particle size and detecting the presence of intact chains of bacterial magnetite. All of the samples measured displayed a Verwey transition (Fig. F1), indicative of magnetite. We did not observe any salient features consistent with mag-

F1. Thermal demagnetization of a low-temperature saturation isothermal remanence, p. 6.

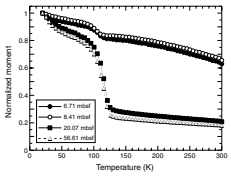

netic iron sulfides. However, greigite (Fe_3S_4) has no low-temperature transitions. Although magnetite is present throughout Site 1096, we observed several differences in the samples taken from above and below 18 mbsf. Samples collected from above 18 mbsf display the Verwey transition at ~103–108 K. M_R decreases by 10%–15% across the Verwey transition, and the field cooled curve is higher than the zero field cooled curve (Fig. **F2A**). These samples show a continuing loss of remanence from 120 K up to room temperature, which could indicate particles with blocking temperatures at or near room temperature. Such particles sizes would be near the transition from superparamagnetic to stable single-domain (SSD) behavior at room temperature. The Verwey transition temperature observed in these samples is lower than values reported for stoichiometric magnetite. Previous studies have reported that oxidation of magnetite lowers, broadens, and suppresses the Verwey transition, as does nonstoichimometry resulting from the substitution of impurities such as Ti, Al, and Mn (Aragón et al., 1993; Özdemir et al., 1993; Kakol et al., 1994). Our observations may be indicative of some degree of cation substitution or nonstoichiometry. Samples from below 18 mbsf display the Verwey transition at 116–120 K (Fig. **F1**). M_R decreases by 50%–60% across the Verwey transition. Further, the field cooled curve is lower than the zero field cooled curve (Fig. **F2B**). This is unexpected because cooling in the presence of a field should bias one of the (100) easy axes of magnetization upon cooling through the Verwey transition. However, this behavior has been observed in several natural and synthetic magnetite samples, and it appears to be a characteristic of multidomain magnetite larger than ~10–14 µm (Brachfeld et al., submitted **[N1]**).

Moskowitz et al. (1993) defined parameter δ_{FC}/δ_{ZFC}, where δ is given by

$$\delta = (M_R[80\ K] - M_R[150\ K])/M_R[80\ K].$$

Moskowitz et al. (1993) observed that intact chains of bacterial magnetite yielded δ_{FC}/δ_{ZFC} values >2. Mixed assemblages and assemblages containing nonbiogenic SSD particles had δ_{FC}/δ_{ZFC} values between 1 and 2. Synthetic pseudosingle domain (PSD) particles had δ_{FC}/δ_{ZFC} values near 1. Samples from above 18 mbsf have δ_{FC}/δ_{ZFC} values of 1.4–1.5, whereas those from below 18 mbsf are <1. We cannot conclusively identify bacterial magnetite by this test alone. However, our observations are consistent with a shift in the magnetic mineral assemblage at 18 mbsf. Hysteresis parameters from Site 1096 form a diffuse cluster that spans the boundary between the PSD and multidomain (MD) region of a Day plot (Day et al., 1977) (Fig. **F3**). Samples from Cores 1H and 2H from each of Holes 1096A and 1096B form a subcluster that plots slightly higher and to the left within the main cluster. However, samples with higher than average ratios of saturation remanence to saturation magnetization (M_R/M_S) occur approximately every 50–100 m down to the base of Hole 1096C.

The average value of the coercivity of remanence (H_{CR}) shifts abruptly at 18 mbsf (Fig. **F4**; Table **T1**). Values of H_{CR} for samples above 18 mbsf are higher than those reported for SSD stoichiometric magnetite (Heider et al., 1996, and references therein). H_{CR} values for titanomagnetites may be elevated by high defect concentrations that pin domain walls or by cation substitution that increases crystalline anisotropy (Day et al., 1977; Readman and O'Reilly, 1972). Very high values of H_{CR}

F2. ZFC and FC curves, p. 7.

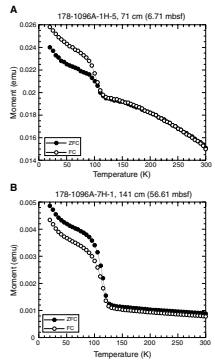

F3. Hysteresis parameters displayed on a Day plot, p. 8.

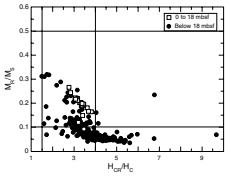

F4. Mg, SO_4, H_{CR}, and χ_{HF}, p. 9.

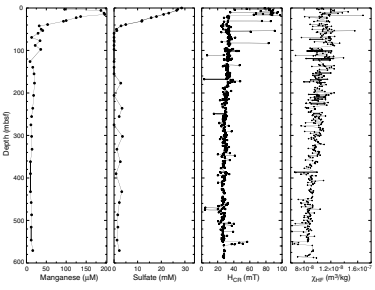

T1. Magnetic hysteresis parameters, Site 1096 p. 10.

have also been reported for SSD greigite (Fe_3S_4), which has high magnetocrystalline anisotropy (Roberts, 1995; Snowball, 1997).

The location of this shift in magnetic granulometry does not correspond to lithologic boundaries. There may be a correlation with geochemical boundaries. The location of the iron reduction boundary is not confidently identified at Site 1096. Iron concentrations were consistently zero in the interstitial water samples. The concentration of dissolved manganese increases from 0 to 15 mbsf, likely resulting from the dissolution of Mn oxides (Fig. **F4**). The bases of the Mn and sulfate reduction zones are at 60 mbsf. It is possible that we are observing the dissolution of fine-grained iron oxides, leaving a coarser residual assemblage below 18 mbsf. Alternatively, we may be seeing the presence of authigenic iron oxides and/or iron sulfides, possibly biogenic in origin, which form in the interval between 0 and 18 mbsf.

SUMMARY

Site 1096 displays a two-part rock-magnetic stratigraphy, with a shift in the magnetic mineral assemblage occurring at 18 mbsf. The assemblage above 18 mbsf consists of magnetite and a second high-coercivity phase. The origin of these particles may be detrital or biogenic. Direct observation of these particles via electron spectroscopy (scanning or transmission electron microscopy) is needed to explore whether some combination of composition (oxide vs. sulfide), oxidation, nonstoichiometry, cation substitution, or high defect concentration is responsible for the high values of H_{CR}. Below 18 mbsf, the assemblage consists of relatively coarser PSD and MD magnetite grains. High-field susceptibility indicates a factor of two dilution of the ferromagnetic particles over the 608-m section (Fig. **F4**). We find that the recording assemblage is very uniform below 18 mbsf.

ACKNOWLEDGMENTS

We thank the crew of the *JOIDES Resolution* and the members of the Leg 178 scientific party for their assistance and discussions. We thank Leonardo Sagnotti for his careful review of this manuscript. This work was funded by a grant from the Joint Oceanographic Institutes/U.S. Science Support Program.

REFERENCES

Aragón, R., Gehring, P.M., and Shapiro, S.M., 1993. Stoichiometry, percolation, and Verwey ordering in magnetite. *Phys. Rev. Lett.,* 70:1635–1638.

Barker, P.F., Camerlenghi, A., Acton, G.D., et al., 1999. *Proc. ODP, Init. Repts.,* 178 [CD-ROM]. Available from: Ocean Drilling Program, Texas A&M University, College Station, TX 77845-9547, U.S.A.

Day, R., Fuller, M., and Schmidt, V.A., 1977. Hysteresis properties of titanomagnetites: grain-size and compositional dependence. *Phys. Earth Planet. Inter.,* 13:260–267.

Dunlop, D.J., and Özdemir, Ö., 1997. *Rock Magnetism: Fundamentals and Frontiers:* Cambridge (Cambridge Univ. Press).

Guyodo, Y., and Valet, J.-P., 1996. Relative variations in geomagnetic intensity from sedimentary records: the past 200,000 years. *Earth. Planet. Sci. Lett.,* 143:23–36.

Guyodo, Y., and Valet, J.-P., 1999. Global changes in intensity of the earth's magnetic field during the past 800 kyr. *Nature,* 399:249–252.

Heider, F., Zitzelberger, A., and Fabian, K., 1996. Magnetic susceptibility and remanent coercive force in grown magnetite crystals from 0.1 µm to 6 mm. *Phys. Earth Planet. Inter.,* 93:239–256.

Kakol, Z., Sabol, J., Strickler, J., Kozlowsiki, A., and Honig, J.M., 1994. Influence of titanium doping on the magnetocrystalline anisotropy of magnetite. *Phys. Rev. B.,* 49:12767–12772.

Laj, C., Kissel, C., Mazaud, A., Channell, J.E.T, and Beer, J., 2000. North Atlantic paleointensity stack since 75 ka (NAPIS-75) and the duration of the Laschamp event. *Phil. Trans. R. Soc. Lond. A,* 358:1009–1025.

Moskowitz, B.M., Frankel, R.B., and Bazylinski, D.A., 1993. Rock magnetic criteria for the detection of biogenic magnetite. *Earth Planet. Sci. Lett.,* 120:283–300.

Özdemir, Ö., Dunlop, D.J., and Moskowitz, B.M., 1993. The effect of oxydation on the Verwey transition in magnetite. *Geophys. Res. Lett.,* 20:1671–1674.

Pudsey, C.J., and Camerlenghi, A., 1998. Glacial-interglacial deposition on a sediment drift on the Pacific margin of the Antarctic Peninsula. *Antarct. Sci.,* 10:286–308.

Readman, P.W., and O'Reilly, W., 1972. Magnetic properties of oxidized (cation-deficient) titanomagnetites $(Fe,Ti)_3O_4$. *J. Geomagn. Geoelectr.,* 24:69–90.

Roberts, A.P., 1995. Magnetic properties of sedimentary greigite (Fe_3S_4). *Earth Planet. Sci. Lett.,* 134:227–236.

Snowball, I.F., 1997. The detection of single-domain greigite (Fe_3S_4) using rotational remanent magnetization (RRM) and the effective gyro field (Bg): mineral magnetic and paleomagnetic applications. *Geophys. J. Int.,* 130:704–716.

Tauxe, L., 1993. Sedimentary records of relative paleointensity of the geomagnetic field: theory and practice. *Rev. Geophys.,* 31:319–354.

Figure F1. The thermal demagnetization of a low-temperature saturation isothermal remanence (M_R) imparted at 20 K. The Verwey transition is observed throughout Site 1096.

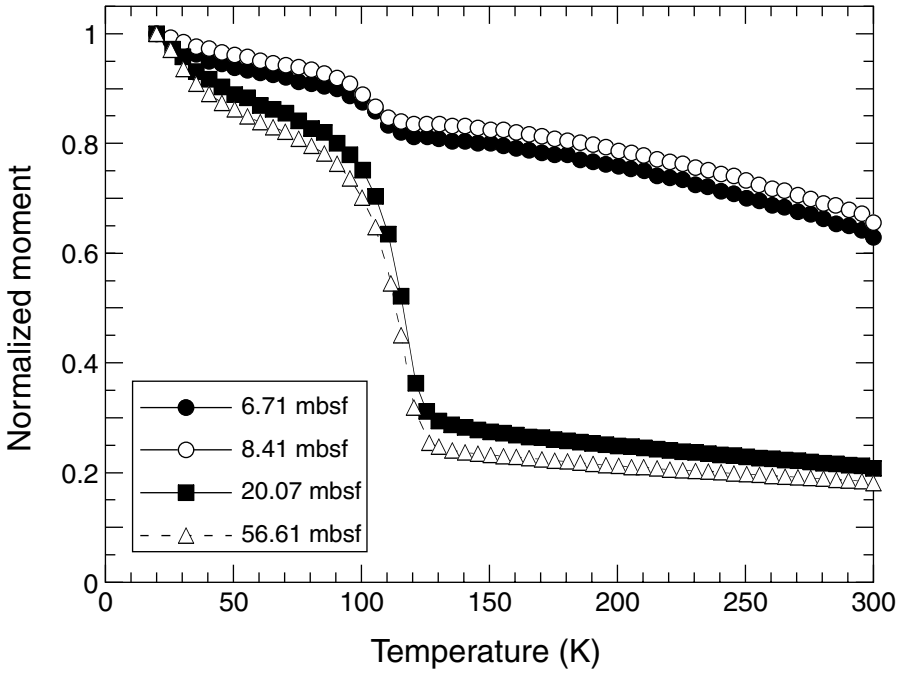

Figure F2. A. Zero field cooled (ZFC) and field cooled (FC) M_R-T curves for Sample 178-1096A-1H-5, 71 cm (6.71 mbsf). The FC curve is higher than the ZFC curve, consistent with SSD particles, possibly of biogenic origin. **B.** ZFC-FC curves for Sample 178-1096A-7H-1, 141 cm (56.61 mbsf). The ZFC curve is lower than the FC curve, consistent with MD magnetite.

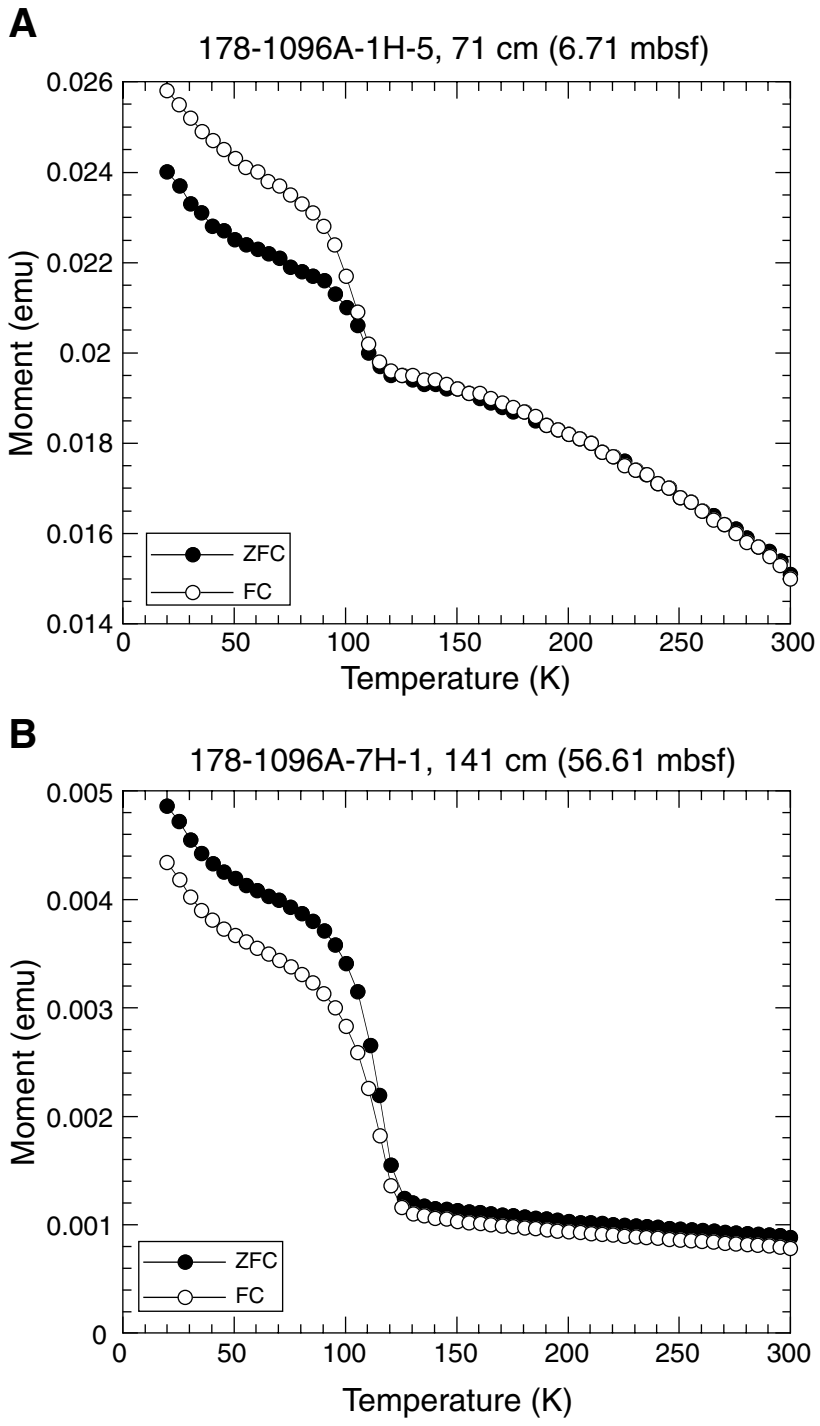

Figure F3. Hysteresis parameters from Site 1096 displayed on a Day plot (Day et al., 1977). Open symbols denote samples from 0 to 18 mbsf. Closed symbols denote samples from below 18 mbsf. M_R = saturation remanence, M_S = saturation magnetization, H_{CR} = coercivity of remanence, H_C = coercivity.

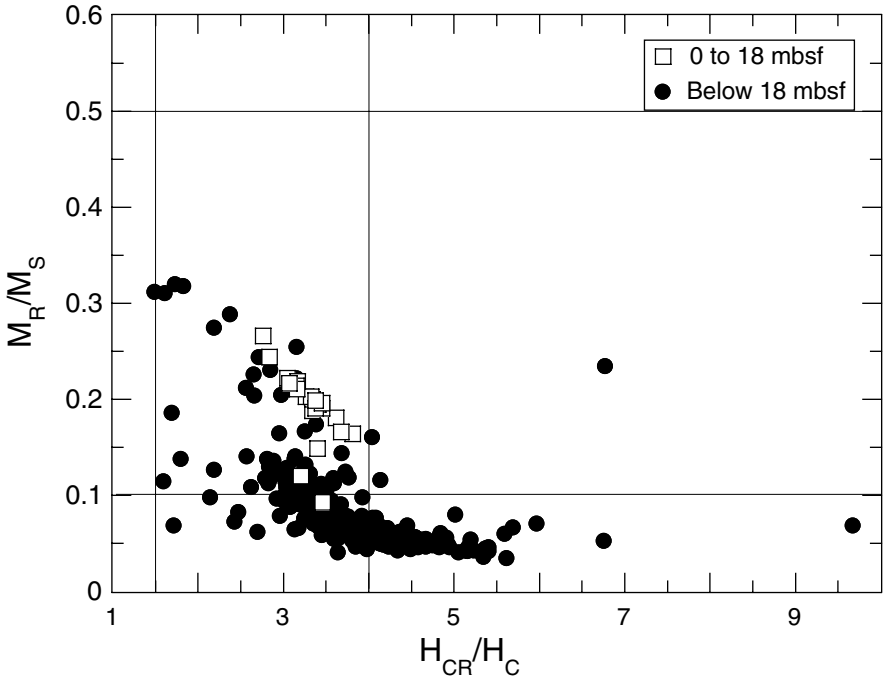

Figure F4. Interstitial water dissolved manganese and sulfate and rock-magnetic parameters H_{CR} and high-field susceptibility (χ_{HF}) from Site 1096. A shift in the magnetic mineral assemblage at 18 mbsf is not clearly correlated with redox zones. However, the increase in dissolved Mn from 0 to 15 mbsf suggests dissolution of Mn oxides. Iron oxides may be dissolving as well.

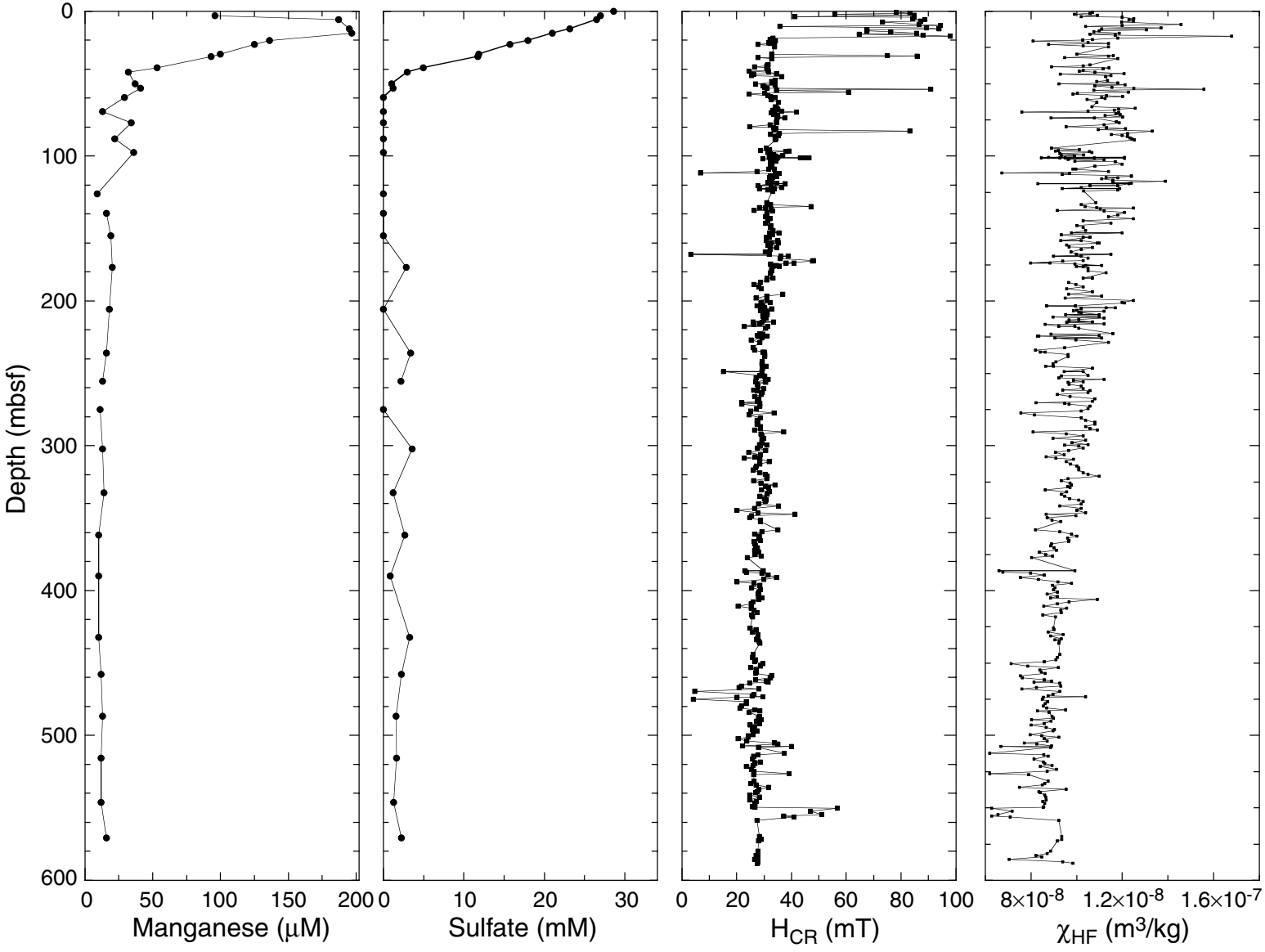

Table T1. Magnetic hysteresis parameters, Site 1096. (See table notes. Continued on next page.)

Core, section, interval (cm)	M_s (Am^2/kg)	M_r (Am^2/kg)	H_c (mT)	H_{cr} (mT)	M_r/M_s	H_{cr}/H_c	χ_{hf} (m^3/kg)
178-1096A-							
1-1H, 2-3	0.141	0.025	17	58.7	0.175	3.45	1.11E–07
1-1H, 70-72	0.193	0.036	23.43	78.26	0.188	3.34	1.07E–07
1-1H, 133-135	0.3	0.054	22.96	83.16	0.181	3.62	1.06E–07
1-2H, 70-72	0.102	0.015	16.44	55.91	0.149	3.4	9.91E–08
1-2H, 143-145	0.139	0.028	25.38	84.83	0.2	3.34	1.09E–07
1-3H, 70-72	0.204	0.024	12.86	41.25	0.12	3.21	1.02E–07
1-3H, 125-127	0.352	0.067	24.55	84.81	0.191	3.45	1.20E–07
1-4H, 70-72	0.279	0.057	25.8	84.3	0.203	3.27	1.25E–07
1-4H, 140-142	0.356	0.069	26.03	88.81	0.195	3.41	1.23E–07
1-5H, 70-72	0.32	0.065	26.2	87.1	0.203	3.32	1.25E–07
1-6H, 50-52	0.251	0.048	21.7	73.3	0.191	3.38	1.20E–07
2-1H, 69-71	0.374	0.073	25.7	88.5	0.196	3.44	1.36E–07
2-1H, 138-140	0.291	0.065	28.4	86.6	0.222	3.05	1.46E–07
2-2H, 70-72	0.237	0.052	29.83	94.51	0.219	3.17	1.20E–07
2-2H, 145-147	0.344	0.032	10.36	35.84	0.093	3.46	1.04E–07
2-3H, 70-72	0.166	0.044	32.3	89.2	0.266	2.76	1.37E–07
2-3H, 136-138	0.237	0.051	29.77	93.92	0.214	3.15	1.11E–07
2-4H, 70-72	0.228	0.048	21.4	67.6	0.211	3.16	1.31E–07
2-4H, 145-147	0.212	0.035	17.7	67.5	0.164	3.81	1.10E–07
2-5H, 45-47	0.19	0.037	22.1	76.3	0.196	3.45	1.08E–07
2-5H, 138-140	0.244	0.049	25.4	85.8	0.199	3.38	1.19E–07
2-6H, 49-51	0.198	0.033	17.6	64.7	0.166	3.68	1.06E–07
2-6H, 102-103	0.151	0.027	18.2	63.5	0.18	3.49	1.22E–07
2-6H, 143-145	0.272	0.059	28.72	88.07	0.217	3.07	1.17E–07
2-7H, 66-68	0.275	0.067	34.53	97.88	0.244	2.83	1.68E–07
3-1H, 144-146	0.35	0.03	9.62	33.27	0.086	3.46	1.18E–07
3-2H, 70-72	0.263	0.022	9.46	32.24	0.086	3.41	1.07E–07
3-2H, 136-138	0.302	0.029	9.53	32.2	0.096	3.38	1.03E–07
3-3H, 46-48	0.146	0.018	11.52	34.18	0.123	2.97	8.10E–08
3-3H, 142-144	0.301	0.03	10.25	31.58	0.101	3.08	1.05E–07
3-4H, 70-72	0.125	0.012	9.69	32.12	0.092	3.31	1.14E–07
3-4H, 137-139	0.088	0.005	5.75	27.7	0.056	4.82	8.78E–08
3-5H, 70-72	0.265	0.027	10.82	33.74	0.1	3.12	1.03E–07
3-5H, 145-147	0.347	0.035	10.65	33.72	0.1	3.17	1.14E–07
4-2H, 140-142	0.204	0.025	11.39	32.64	0.121	2.87	1.00E–07
4-3H, 140-142	0.153	0.035	30.19	85.83	0.231	2.84	1.14E–07
4-3H, 85-87	0.16	0.036	23.8	75.1	0.222	3.16	1.16E–07
4-4H, 70-72	0.133	0.076	6.11	27.76	0.057	4.54	9.49E–08
4-4H, 140-142	0.221	0.022	10.65	32.74	0.1	3.07	1.18E–07
5-1H, 70-72	0.265	0.024	9.25	31.48	0.089	3.4	1.06E–07
5-1H, 144-146	0.181	0.016	9.06	31.02	0.088	3.42	1.03E–07
5-2H, 70-72	0.068	0.004	5.68	26.52	0.055	4.67	8.90E–08
5-2H, 140-142	0.304	0.026	8.91	31.4	0.086	3.52	1.14E–07
5-3H, 70-72	0.092	0.008	8.59	30.9	0.084	3.6	1.12E–07
5-3H, 140-142	0.282	0.026	9.41	31.45	0.091	3.34	1.03E–07
5-4H, 70-72	0.033	0.002	5.12	24.6	0.049	4.8	1.01E–07
5-4H, 140-142	0.003	0.381	8.51	31.7	0.125	3.73	1.08E–07
5-5H, 70-72	0.25	0.028	11.4	34.5	0.114	3.03	1.21E–07
5-5H, 140-142	0.02	0.001	5.87	26.1	0.065	4.45	9.29E–08
5-6H, 69-71	0.002	0.344	15	25.4	0.186	1.69	1.15E–07
5-6H, 140-142	0.003	0.484	10.8	36.5	0.174	3.38	1.13E–07
6-2H, 80-82	0.184	0.018	10.2	33.9	0.097	3.32	1.14E–07
6-2H, 140-142	0.336	0.033	10	32.8	0.097	3.28	1.09E–07
6-3H, 80-82	0.374	0.04	10.8	32.9	0.106	3.05	1.18E–07
6-3H, 140-142	0.012	0.816	4.51	26.9	0.071	5.96	9.22E–08
6-4H, 76-78	0.263	0.029	11.2	34	0.109	3.04	1.21E–07
6-4H, 140-142	0.164	0.016	9.73	29.7	0.099	3.05	1.08E–07
6-5H, 78-80	0.194	0.019	9.8	30.3	0.096	3.09	1.15E–07
6-5H, 140-142	0.182	0.021	11.2	31.2	0.118	2.79	1.25E–07
6-6H, 78-80	0.254	0.073	38.3	90.9	0.289	2.37	1.56E–07
6-6H, 138-140	0.283	0.03	10.9	34.5	0.105	3.17	1.08E–07
7-1H, 70-72	0.132	0.027	20.5	60.9	0.205	2.97	1.23E–07
7-1H, 140-142	0.109	0.008	7.42	30.3	0.077	4.08	1.00E–07
7-2H, 60-62	0.036	0.001	4.38	24.6	0.035	5.62	9.84E–08
7-2H, 142-144	0.092	0.007	7.99	31.3	0.079	3.92	1.13E–07
7-3H, 70-72	0.196	0.019	10.4	32.4	0.097	3.12	1.20E–07
7-3H, 140-142	0.123	0.011	10.9	33.9	0.09	3.11	1.11E–07

Table T1 (continued).

Core, section, interval (cm)	M_s (Am^2/kg)	M_r (Am^2/kg)	H_c (mT)	H_{cr} (mT)	M_r/M_s	H_{cr}/H_c	χ_{hf} (m^3/kg)
7-4H, 68-70	0.197	0.018	10	32.7	0.093	3.27	1.12E–07
7-4H, 140-142	0.124	0.012	9.87	32.5	0.094	3.29	1.05E–07
7-6H, 60-62	0.002	0	19.6	35.2	0.138	1.8	1.09E–07
8-1H, 138-140	0.083	0.008	10.3	34.2	0.092	3.32	1.07E–07
8-2H, 70-72	0.332	0.034	11.2	34.6	0.102	3.09	1.26E–07
8-2H, 140-142	0.237	0.025	11.3	35	0.104	3.1	1.18E–07
8-3H, 74-76	0.319	0.029	9.49	33.3	0.092	3.51	1.16E–07
8-3H, 134-136	0.002	0	5.39	36.5	0.235	6.77	1.05E–07
8-4H, 74-76	0.264	0.022	9.08	32.5	0.082	3.58	1.19E–07
8-4H, 138-140	0.303	0.028	9.75	33.7	0.093	3.46	1.17E–07
8-5H, 76-78	0.271	0.028	10.5	33.4	0.104	3.18	1.19E–07
8-5H, 140-142	0.235	0.024	10.6	34.9	0.101	3.29	1.13E–07
8-6H, 80-82	0.294	0.031	10.9	35	0.105	3.21	1.20E–07
8-6H, 140-142	0.002	0	23.3	34.7	0.312	1.49	1.08E–07
9-2H, 70-72	0.276	0.029	10.9	34.6	0.105	3.17	1.17E–07
9-2H, 126-128	0.292	0.03	10.9	34.5	0.102	3.17	1.19E–07
9-5H, 68-70	0.004	0	10	24.7	0.083	2.47	9.55E–08
9-5H, 140-142	0.191	0.025	11.8	33.4	0.13	2.83	1.13E–07
9-6H, 70-72	0.238	0.029	11.6	34.3	0.123	2.96	1.22E–07
9-6H, 130-132	0.15	0.021	12	33.7	0.138	2.81	1.09E–07
9-7H, 98-100	0.297	0.073	30.7	83.2	0.244	2.71	1.33E–07
10-1H, 70-72	0.178	0.019	11.2	35.6	0.106	3.18	1.22E–07
10-1H, 140-142	0.122	0.009	7.99	32.3	0.077	4.04	1.15E–07
10-2H, 140-142	0.164	0.016	10.2	35.2	0.1	3.45	1.20E–07
10-2H, 144-146	0.187	0.019	10.3	34.2	0.1	3.32	1.22E–07
10-3H, 70-72	0.181	0.017	9.89	34.3	0.095	3.47	1.23E–07
10-3H, 138-140	0.198	0.019	10.3	33.9	0.097	3.29	1.24E–07
10-4H, 70-72	0.222	0.022	10.5	34.1	0.098	3.25	1.25E–07
11-1H, 139-141	0.108	0.008	8.13	30.7	0.074	3.78	8.91E–08
11-2H, 69-71	0.152	0.013	9.06	32	0.085	3.53	1.01E–07
11-2H, 141-143	0.024	0.001	5.51	28.6	0.054	5.19	9.21E–08
11-3H, 70-72	0.002	0	17.4	38	0.127	2.18	1.06E–07
11-3H, 142-144	0.099	0.008	8.46	31.3	0.079	3.7	1.07E–07
11-4H, 70-72	0.292	0.025	9.24	32.2	0.086	3.48	9.27E–08
11-4H, 143-145	0.27	0.026	10.3	33.5	0.096	3.25	1.03E–07
11-5H, 70-72	0.308	0.032	10.9	34.1	0.103	3.13	9.90E–08
11-5H, 145-147	0.33	0.03	9.83	33.1	0.091	3.37	9.91E–08
11-6H, 13-15	0.003	0	21.9	35	0.115	1.6	8.77E–08
11-6H, 41-43	0.002	0	20.3	44.4	0.275	2.19	9.26E–08
11-6H, 43-45	0.003	0	8.3	46.4	0.06	5.59	8.44E–08
11-6H, 46-48	0.003	0	13.8	43.2	0.138	3.13	1.08E–07
11-6H, 70-72	0.278	0.027	10.2	33.4	0.095	3.27	9.50E–08
11-6H, 94-96	0.322	0.033	10.9	34.7	0.103	3.18	1.21E–07
11-6H, 143-145	0.253	0.025	10.3	33.4	0.098	3.24	9.63E–08
12-1H, 92-94	0.221	0.023	10.8	34.3	0.102	3.18	9.93E–08
13-1H, 49-51	0.239	0.023	10.4	34.2	0.097	3.29	9.36E–08
13-1H, 88-90	0.035	0.004	12.1	34.1	0.113	2.82	9.71E–08
14-1H, 80-82	0.288	0.028	10.2	33.6	0.096	3.29	9.37E–08
14-2H, 79-81	0.1	0.01	10.5	33	0.103	3.14	1.03E–07
15-1H, 97-99	0.014	0.001	6.16	30.9	0.08	5.02	1.08E–07
15-2H, 70-72	0.003		12.2	32.4	0.204	2.66	1.02E–07
15-3H, 50-52	0.002		4.87	47.1	0.069	9.67	1.04E–07
15-3H, 143-145	0.004		16.5	28.3	0.069	1.72	1.09E–07
15-4H, 90-92	0.313	0.027	9.27	32.6	0.085	3.52	1.10E–07
15-5H, 80-82	0.397	0.034	9.11	33	0.086	3.62	1.12E–07

Notes: M_s = saturation magnetization, M_r = saturation remanence, H_{cr} = coercivity of remanence, H_c = coercivity, χ_{hf} = high-field magnetic susceptibility. Only a portion of this table appears here. The complete table is available in **ASCII**.

CHAPTER NOTE*

N1. Brachfeld, S., Banerjee, S.K., Guyodo, Y., and Acton, G.D., submitted. A 13,000 year history of century to millennial scale environmental oscillations magnetically recorded in the Palmer Deep, western Antarctic Peninsula. *Earth Planet. Sci. Lett.*

30 January 2002: Brachfeld, S.A., Banerjee, S.K., Guyodo, Y., and Acton, G.D., 2002. A 13,000 year history of century to millennial-scale paleoenvironmental change magnetically recorded in the Palmer Deep, western Antarctic Peninsula. *Earth Planet. Sci. Lett.,* 194:311–326.

*Dates reflect file corrections or revisions.